



3 4456 0268430 7

ORNL/TM-10643

ornl

**OAK RIDGE
NATIONAL
LABORATORY**

MARTIN MARIETTA

Ion Microprobe Mass Spectrometry Using Sputtering Atomization and Resonance Ionization: Final Report

D. E. Goeringer
W. H. Christie
L. K. Bertram
R. L. Walker
J. A. Carter

OAK RIDGE NATIONAL LABORATORY
CENTRAL RESEARCH LIBRARY
CIRCULATION SECTION
4400N ROOM 173
LIBRARY LOAN COPY
DO NOT TRANSFER TO ANOTHER PERSON
If you wish someone else to see this
report, send to room with report and
the library will arrange a loan.

OPERATED BY
MARTIN MARIETTA ENERGY SYSTEMS, INC.
FOR THE UNITED STATES
DEPARTMENT OF ENERGY

Printed in the United States of America. Available from
National Technical Information Service
U. S. Department of Commerce
5285 Port Royal Road, Springfield, Virginia 22161
NTIS price codes—Printed Copy, A03; Microfiche A01

This report was prepared as an account of work sponsored by an agency of the United States Government. Neither the United States Government nor any agency thereof, nor any of their employees, makes any warranty, express or implied, or assumes any legal liability or responsibility for the accuracy, completeness, or usefulness of any information, apparatus, product, or process disclosed, or represents that its use would not infringe privately owned rights. Reference herein to any specific commercial product, process, or service by trade name, trademark, manufacturer, or otherwise, does not necessarily constitute or imply its endorsement, recommendation, or favoring by the United States Government or any agency thereof. The views and opinions of authors expressed herein do not necessarily state or reflect those of the United States Government or any agency thereof.

Contract NO. DE-AC05-84OR21400

Analytical Chemistry Division

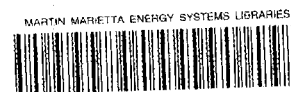
ION MICROPROBE MASS SPECTROMETRY
USING SPUTTERING ATOMIZATION AND
RESONANCE IONIZATION:
FINAL REPORT

by

D. E. Goeringer, W. H. Christie, L. K. Bertram,
R. L. Walker, and J. A. Carter

Date Published: December 1987

OAK RIDGE NATIONAL LABORATORY
Oak Ridge, Tennessee 37831
operated by
Martin Marietta Energy Systems, Inc.
for the
Department of Energy



3 4456 0268430 7

Table of Contents

	Page
Abstract	1
1. Introduction	3
2. Experimental	5
2.1 IMMA	5
2.2 Ion Optics	5
2.3 Laser Source and Light Optics	6
2.4 Signal Processing	8
2.5 Data Acquisition/Control System	9
2.6 Optical and Mass Spectra	11
2.7 Sputter Yield Measurements	13
2.8 Samples	14
3. Results and Discussion	15
3.1 Sputter Yields	15
3.2 RIMS of Uranium	15
3.3 Depth Profiling	21
3.4 Pulsed Primary Ion Beam	25
3.5 SIMS and RIMS Comparisons	28
3.6 <u>In Situ</u> Reduction	30
3.7 Numerical Estimates	32
4. Conclusion	35
References	37

List of Figures

<u>Figure</u>	<u>Title</u>	<u>Page</u>
1	Modified ion optics to extract photoions produced in a volume above the sample surface	7
2	Electronics for SA/RIMS data acquisition/control using an LSI-11/2 microcomputer	10
3	Electronics for SA/RIMS data acquisition/control using a MicroPDP-11 microcomputer	12
4	Optical ionization spectra obtained with a flashlamp-pumped dye laser for ^{238}U atoms produced by ion beam sputtering (top) and thermal filament atomization (bottom)	16
5	Optical ionization spectrum obtained with a Nd:YAG-pumped dye laser for ^{238}U atoms produced by ion beam sputtering	18
6	Mass spectra of photoions produced via laser post-ionization of ion-beam-sputtered uranium	19
7	Optical spectrum for production of UO^+ photoions	20
8	Time (depth) profiles of mass-selected ions produced by ion-beam sputtering of U metal covered with a thin UO_2 film: * - U^+ , o - UO^+ , + - UO_2^+	23
9	Time (depth) profiles of mass-selected ions produced by laser ionization of neutrals sputtered from U metal covered with a thin UO_2 film: * - U^+ , o - UO^+ , + - UO_2^+	24
10	Time response of the laser ionization signal for U^+ from U metal sputtered with a pulsed Ar^+ beam of varying pulse duration: + - 5 s, o - 200 s	26
11	Time response of the laser ionization signals for UO^+ and UO_2^+ from U metal alternately sputtered with a 5 s duration pulsed and cw Ar^+ beam: o - UO^+ , + - UO_2^+	27

Ion Microprobe Mass Spectrometry
Using Sputtering Atomization and
Resonance Ionization:
Final Report

D. E. Goeringer, W. H. Christie, L. K. Bertram,
R. L. Walker, and J. A. Carter

Abstract

Resonance ionization mass spectrometry (RIMS) utilizing ion beam sputtering has been applied to the measurement of U. The goal is to produce an ultra sensitive technique for analysis of small environmental particles. The method has also been compared with secondary ion mass spectrometry (SIMS). Samples studied were uranium metal, UO_2 (polycrystalline and single crystal), and U_3O_8 . The overall efficiency of detection for sputter atomization/resonance ionization mass spectrometry (SA/RIMS), U^+ photoions counted/U atoms sputtered, was approximately 9×10^{-4} . Results indicate that the density of ground-state U atoms sputtered from such samples is quite sensitive to oxygen content and surface contamination. The relative ratio of ground-state U atoms sputtered from U metal and UO_2 ($U^{\circ}_{\text{metal}}/U^{\circ}_{\text{oxide}}$) with Ar^+ was estimated as 4.4×10^1 . This relatively large matrix effect severely limits the applicability of SA/RIMS to quantitative analysis of uranium samples.

1. Introduction

Environmental monitoring of airborne particles for trace levels of uranium is an important problem faced by many government facilities. Depending on particle size and composition, such small samples may contain only femtogram to picogram amounts of uranium in a variety of chemical forms. Therefore, detection and quantification of uranium under these conditions requires a high-sensitivity technique relatively insensitive to the chemical environment.

Although SIMS is without peer as a qualitative surface analytical technique, its quantitative aspects are plagued by wide variations in sputtered ion yields attributed to sample matrix effects. Because the major fraction of secondary particle emission from an ion beam sputtered surface usually consists of neutral atoms and molecules (1), analytical techniques based on post-ionization of desorbed neutrals are believed to be less sensitive to the chemical environment than SIMS. Pulsed laser ionization is an attractive process for coupling with ion beam sputtering because the ionization process can be saturated provided that the laser beam is sufficiently powerful. In addition, when pulsed sputtering is utilized, the spatial overlap between the sputtered plume and laser beam can approach unity. Therefore, efficient laser post-ionization of the more abundant neutral fraction also presents the possibility for enhanced sensitivity. This report describes the use of SA/RIMS as an analytical technique for uranium-containing samples. In some instances, material from an earlier report (2) is included for completeness.

2. Experimental

2.1 IMMA

The Applied Research Laboratories (ARL) ion microprobe mass analyzer (IMMA) used in this work is based on the design of Liebl (3). Modifications to the ion extraction lens system, which aid discrimination against secondary ions while allowing efficient collection of lower energy laser-generated ions, are described in a following section. For this study the secondary mass analyzer was operated at mass resolutions ($M/\Delta M$) on the order of 200. Primary ions were generated by using either pure Ar or a mixed gas consisting of approximately 2 atom % Ar, 34 atom % N_2 , and 64 atom % O_2 in the duoplasmatron ion source. The primary ion beam was pulsed by applying a $\pm 450V$ pulse to opposing alignment plates located at the top of the primary lens column. Ion beam gate duration and delay were set with gate/delay generators triggered by the laser flashlamp sync pulse.

To facilitate the ion optical changes, the indium metal seal used to attach the microscope to the sputtering chamber, was replaced with a large viton o-ring. This provided a vacuum-worthy seal that allowed removal and replacement of the microscope in minutes when access to the sputtering chamber was desired.

The standard 400 l/s ion pump was replaced with a 1200 l/s cryosorption unit; the background pressure was approximately 2×10^{-7} torr. System pressure under typical operating conditions was ca. 5×10^{-7} torr.

2.2 Ion Optics

The existing ion extraction optics of the IMMA instrument were designed to efficiently extract sputtered secondary ions produced at the sample surface. Curvature of the equipotential surfaces in the vicinity of the pickup electrode results in highly efficient steering of the sputtered secondary ions which exit the surface at varying angles up to 45° from the normal and with energies ranging from 0 to 20 eV.

Subsequent energy filtering by the electrostatic sector and mass dispersion in the magnetic sector result in a conventional secondary ion mass spectrum.

Computer simulation (SIMION) shows that photoions produced above the laser surface are affected differently by the field and are deflected too much. Most of them strike the inner surface of the extraction electrode and are lost. Even those which pass through the extraction electrode will have too much angular deviation from the ideal angle (45°) to be refocused by subsequent ion lenses.

Because of the inefficiencies in collecting photoions with the standard extraction electrode, new ion optical designs were also modelled. One of the most successful is shown in Figure 1. The objective was to create a flat extraction field in the volume directly above the sample surface, with the field equipotential surfaces inclined at the desired angle (45°) relative to the sample surface. To achieve this, a "pusher" electrode was added (shown at the right in Figure 1), and the extraction electrode itself was significantly changed. Ions formed in the volume element shown follow a nearly perfect trajectory through the extraction electrode.

2.3 Laser Source and Light Optics

Two different tunable laser systems were evaluated in this study: a flashlamp-pumped dye laser (Chromatix CMX-4) and a Nd:YAG-pumped dye laser (Quanta Ray DCR-2A/PDL-2).

The flashlamp-pumped laser had an optical bandwidth of approximately 3 cm^{-1} and an optical pulse width of about $1 \mu\text{s}$; the Rhodamine-6G dye used in the study produced a useful wavelength range of approximately 580-610 nm. The laser beam was spatially filtered and focused to approximately a 0.05 cm diameter spot directly above the sample with a telescope assembly housing a $10 \mu\text{m}$ pinhole. The pulse energy measured directly at the laser output was about 5 mJ with the available energy above the sample surface estimated to be from 10-50 times less.

The Nd:YAG-pumped laser was operated in fifth order resulting in a bandwidth of approximately 0.3 cm^{-1} . Rhodamine 610 dye used in our

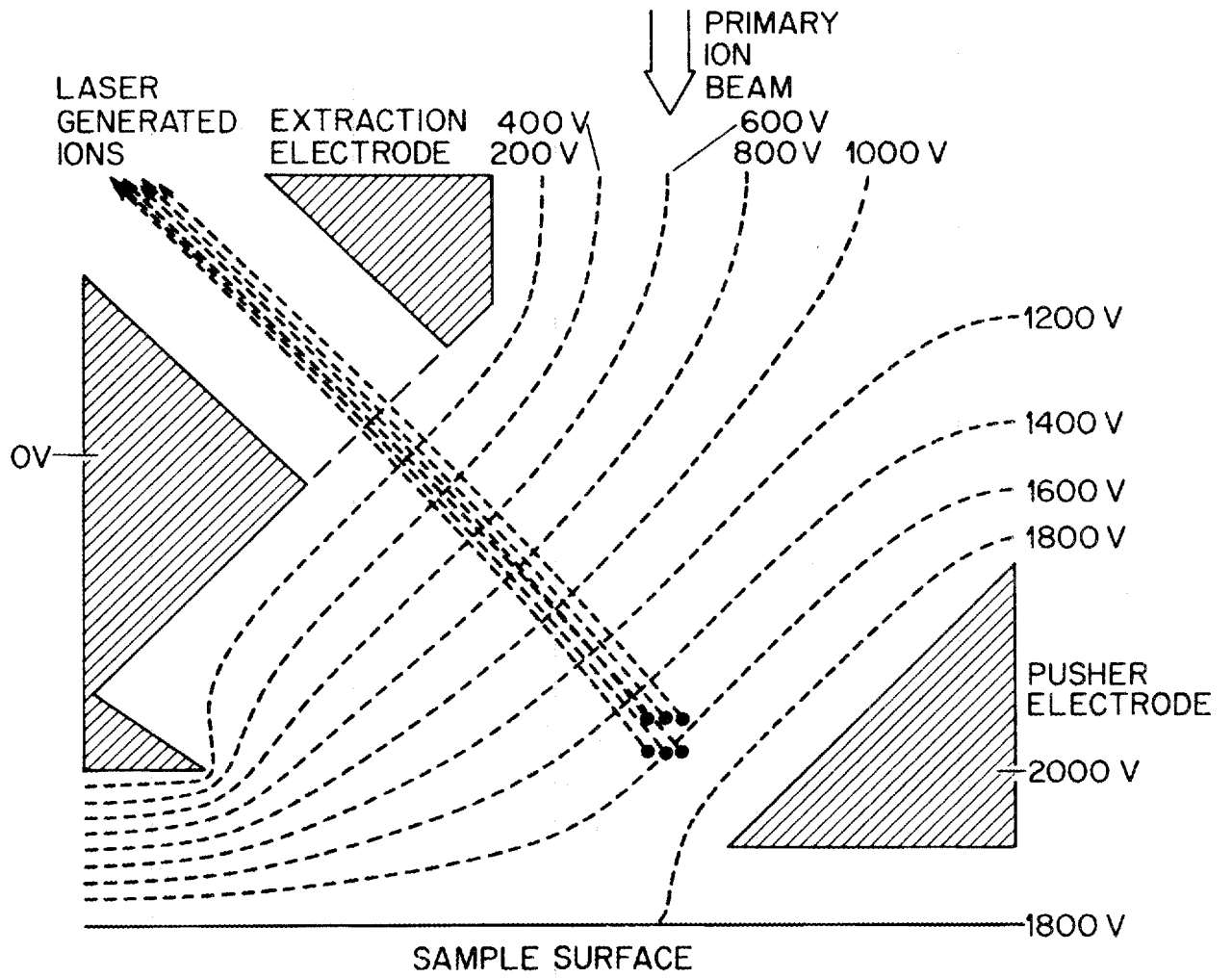


Fig. 1 Modified ion optics to extract photoions produced in a volume above the sample surface.

experiments gave a useful tuning range from about 580-595 nm. The 6-mm diameter beam from the dye laser was collimated to approximately 2 mm via a positive/negative (3:1 focal length ratio) lens telescope system. Typically, 10-12 mJ/pulse of light (measured at the laser output) was used. An estimated 50% of this energy was lost before reaching the sputtered plume.

The laser beam in each case was directed through an optical port at the rear of the IMMA. Due to physical constraints of the IMMA, the plane of the sample surface was several centimeters below that of the laser beam. Therefore, a periscope assembly constructed from two right-angle prisms was mounted inside the sputtering chamber allowing the laser beam to be directed just above and in the plane of the sample.

2.4 Signal Processing

The SIMS signal from cw sputter-ionization and the RIMS signal produced by pulsed resonance ionization (RI) required two different methods of processing. Small, continuous secondary ion currents in our SIMS experiments were well suited for pulse counting with its sensitivity and dynamic range. Therefore, the standard ARL digital system consisting of a discriminator, pre-scaler, and fast pulse counting electronics (pulse-pair resolution of 30 ns) was used for SIMS measurements. Because the duration of the laser pulse for RI was quite short (~10 ns), the packet of photoions arrived at the detector in a very short period of time producing multiple individual pulses that often overlapped. Problems with ion bunching and pulse-pair resolution precluded the use of ion counting with such a RIMS signal, so an analog detection scheme was used. The analog system consisted of a variable-gain, variable-time-constant current amplifier and gated integrator (Stanford Research Systems SR250). The multiple-pulse RIMS signal, generated from a single laser shot, was shaped by the current amplifier (10 μ s time constant) into a single pulse approximately 15 μ s wide and then AC-coupled to the input of the gated integrator. The gated integrator, which was triggered by the laser and for which the gate was delayed for the flight time of the ion packet through the mass spectrometer, then sampled this pulse.

The integrator output was the integral of the input pulse during the gate, normalized by the gate width, i.e., the output was proportional to the average of the input pulse during the sampling gate. Therefore, the integral of the signal pulse (units of V-s), which was proportional to the number of ions contained in the packet, was the DC output of the gated integrator multiplied by the gate width. The DC output from the gated integrator was digitized by an analog-to-digital converter (ADC) in the data system (see below) enabling spectra to be digitally stored. Although the pulse counting system was useful for measuring the magnitude of secondary ion signals, it was not interfaced to the data acquisition computer. Therefore, SIMS spectra were acquired with the data system by increasing the gain and time constant (10 ms) of the current amplifier and DC-coupling its output to the gated integrator. The analog signal from the current amplifier was also used to drive video amplifiers in the standard ARL video display system. Because the Daly detector was wired with both analog and pulse counting outputs, the photomultiplier's signal could be processed simultaneously by both analog and digital electronic systems.

2.5 Data Acquisition/Control System

Initial studies were done with an LSI-11/2-based microcomputer. A schematic diagram of the system is shown in Figure 2. The unit housed a 12-bit analog-to-digital converter (ADC), two digital-to-analog converters (DAC), and a 16-bit parallel I/O interface. The ADC sampled and digitized the DC output from the gated integrator. The direction and speed of a stepping motor attached to the wavelength drive of the flashlamp-pumped laser were controlled by the parallel interface. The DAC outputs were used to drive an x-y scope for real-time display of spectra or an x-y plotter for post-acquisition recording of spectra.

Later work was performed with a microcomputer system (MicroPDP-11) based on an PDP-11/23-Plus (Digital Equipment Corp.) central processing unit. The system contained a 12-bit, combination ADC/dual digital-to-analog converter (DAC) interface board; the ADC digitized the DC output

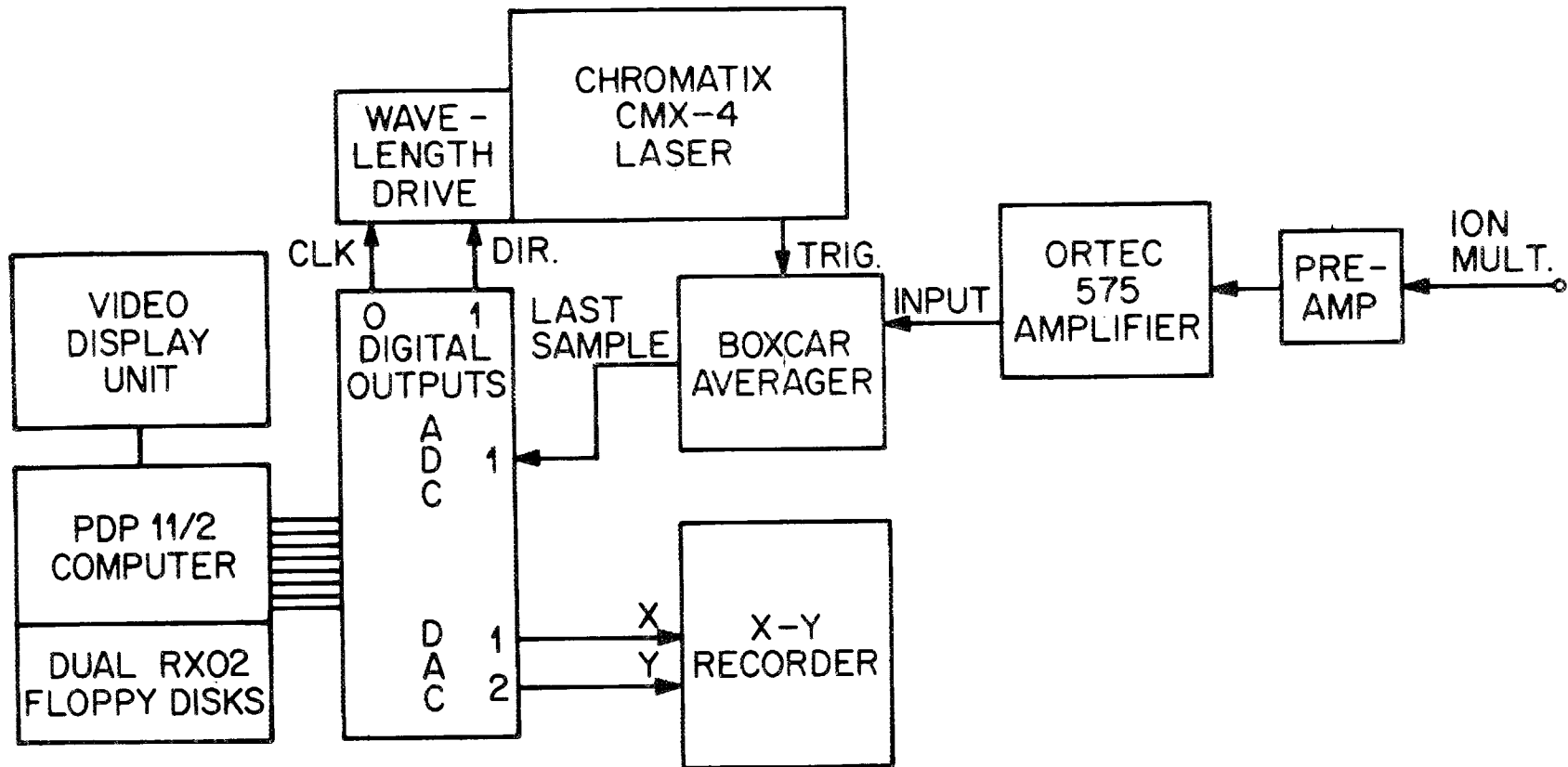


Fig. 2 Electronics for SA/RIMS data acquisition/control using an LSI-11/2 microcomputer.

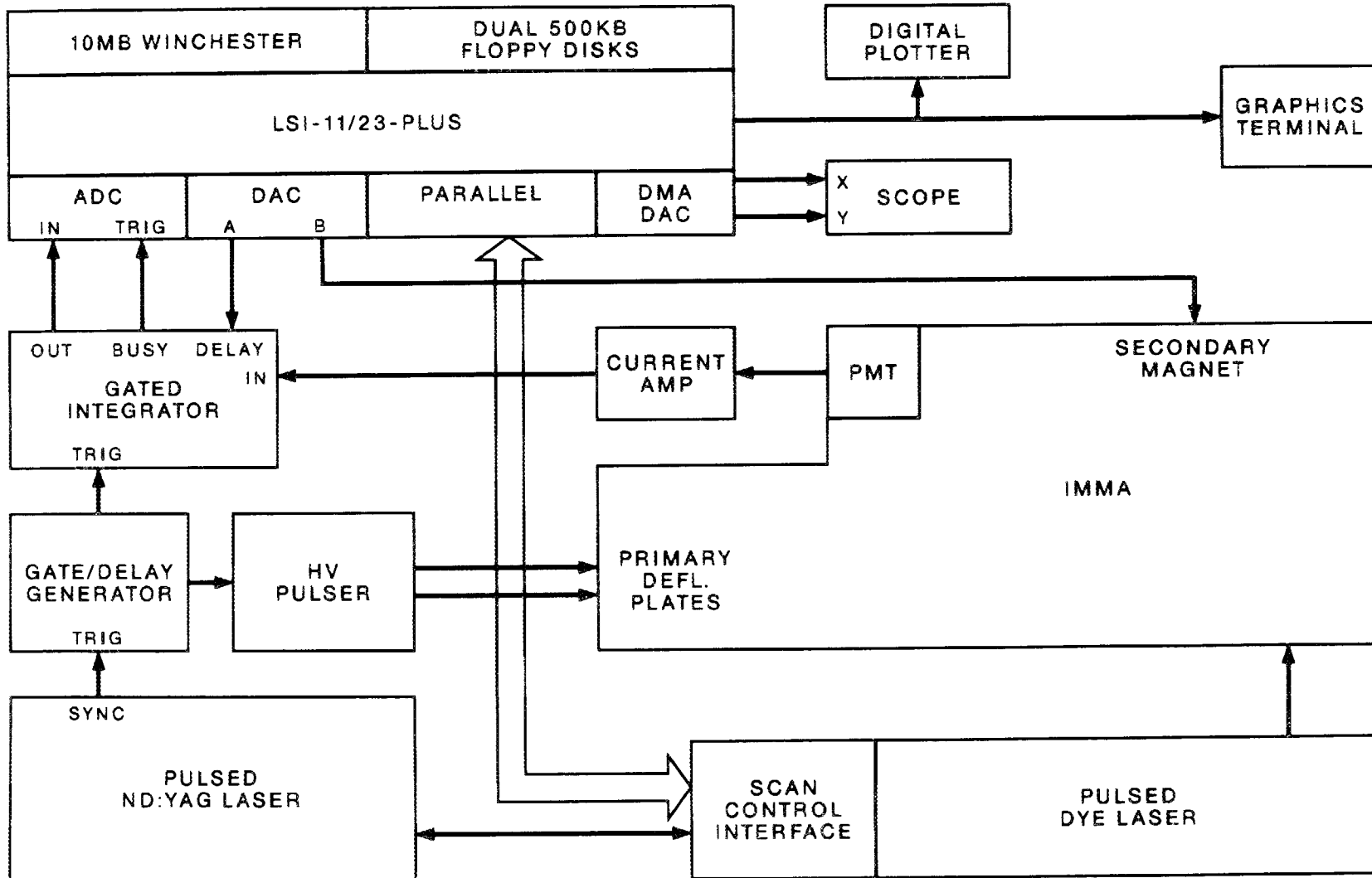
of the gated integrator, and the DACs controlled the secondary magnet as well as the gate delay for the gated integrator. Another DAC with direct memory access capability was used to drive an x-y scope for either real-time or post-processed signal display. Spectra could also be sent to a digital plotter for hard copy output. A parallel interface was used to communicate with the dye laser (Nd:YAG-pumped) motor control interface. A schematic diagram of the complete system is shown in Figure 3.

Modifications were also made to the control electronics to adapt the IMMA for automated particulate analyses. Although the instrument has the capability for primary beam rastering and x-y sample stage movement, it was not designed to facilitate digital computer control of these functions. Therefore, a third dual-output DAC (DMA-controllable) and a multifunction counter-timer (MCT) were also installed in the MicroPDP-11. The DAC performed the functions of driving the raster electronics, firing the laser, and triggering the primary beam gate. The MCT was interfaced to the stage movement electronics enabling the microcomputer to digitally control the stage position. Software was developed which enabled the primary ion beam to raster a $100 \times 100 \mu\text{m}$ area in $10 \mu\text{m}$ increments; the stage would then be translated $100 \mu\text{m}$ along either the x- or y-axis and another raster performed. The area interrogated by this systematic beam raster/stage translation was essentially limited by the range of travel for the stage ($2.5 \times 1.6 \text{ cm}$).

2.6 Optical and Mass Spectra

Using the above computer systems, two types of RIMS spectral data were acquired: 1) optical spectra, which recorded the photoionization signal at a fixed mass as a function of dye laser output wavelength 2) mass spectra, which recorded the photoionization signal at a fixed laser wavelength. Optical data were collected at intervals of 0.027 and 0.06 nm with the flashlamp-pumped and the Nd:YAG-pumped lasers, respectively. Mass spectra were acquired at 0.2 amu intervals. Typically, 15-20 laser shots were averaged for each data point in both types of RIMS spectra, and the spectra were uncorrected for secondary ion signals because of the

DATA ACQUISITION AND CONTROL ELECTRONICS



12

Fig. 3 Electronics for SA/RIMS data acquisition/control using a MicroPDP-11 microcomputer.

effectiveness of the ion extraction optics/time gating in reducing such background. Secondary ion mass spectra were obtained by increasing the sample voltage (secondary mass spectrometer accelerating voltage) and making signal processing adjustments (see above); this permitted secondary ions to be collected by the ion extraction electrode, transmitted through the electrostatic analyzer, and digitized by the data system. The baselines for all spectra were slightly offset (~ 25 units) from zero due to a small DC offset (~ 60 mV) added to the input of the gated integrator. All RIMS and SIMS spectra were acquired with the duoplasmatron source at 16 kV and the sample at a nominal 1500 V resulting in 14.5 keV net primary ion beam energy.

2.7 Sputter Yield Measurements

Sputter yield determinations for different primary ion beams on U metal samples were performed by measuring dimensions of sputter craters with a stylus profilometer (Tencor Alpha-Step 200) having a depth resolution of 50 angstroms. For each determination the primary beam was adjusted to 10 nA and nominally rastered for 15 minutes over a region ~40 x 50 μm . Sputter yields were then calculated from the integrated primary ion current, volume of the sputtered crater, and sample atomic density. Sputter yield determinations for UO_2 used a raster ~80 x 100 μm on a uranium metal alloy (2 w% Zr, 7.5 w% Nb) sample having a relatively uniform (~750 angstrom) layer of UO_2 , grown by oxidation, on its surface. However, surface irregularities on the thin oxide layer precluded accurate profilometric measurement of the depth for sputter craters. Sputter yields, in the case of UO_2 , were estimated by noting the elapsed time between initiation of sputtering and a visual change in the appearance of the sputtered surface indicative of the underlying U alloy. Plots of relative SIMS signal (U^+ , UO^+ , and UO_2^+) versus time also provided an estimate of the time required to sputter through the oxide layer; these sputtering times correlated well with those times noted visually.

2.8 Samples

Samples of U and Sm were prepared by encapsulating specimens of the metal in low vapor pressure epoxy. The top surface of the epoxy mount was ground flat, exposing an area of each metal, and then polished to a mirror finish. After cleaning, the mount was immediately coated with 30-40 nm of carbon to provide electrical conductivity and to protect the metals from oxidation. Several small (1 mm) single crystals of UO_2 were crushed to provide many smaller (50 -200 μm) pieces which were pressed into a flat In metal surface. Specimens prepared in this fashion required no further processing prior to analysis. Finally, U_3O_8 was prepared by heating uranyl nitrate in air. The fine powder produced in this fashion was slurried with water and loaded as a thin film onto a flat pyrolytic carbon planchet. After evaporation of the water, the U_3O_8 was found to adhere to the planchet surface. No further processing of this material was required prior to analysis.

3. Results and Discussion

3.1 Sputter Yields

Results for the sputter yield measurements of U metal, U atoms ejected per incident primary ion, are 5.3, 0.50, and 0.67 for Ar^+ , O_2^+ , and N_2^+ , respectively; the estimated error for the values is $\pm 20\%$. As expected, Ar^+ is far more efficient than N_2^+ and O_2^+ in the number of U atoms ejected from U metal per incident ion. It was also found to be superior for SA/RIMS based on the ratio of U^+ photoion signals observed from U metal ($\text{Ar}^+/3.2 \times 10^2 : \text{N}_2^+/1.5 : \text{O}_2^+/1.0$). Due to its superior secondary ion yields, O_2^+ is generally preferred for inorganic SIMS analyses, but it is less desirable than Ar^+ for SA/RIMS because of its lower atomic neutral yields. The sputter yield for Ar^+ on UO_2 is estimated as 2 ± 0.5 (U atoms/ion). Note that the relative ratio for Ar^+ sputter yields from U metal and UO_2 , 2.7, is within experimental error of the factor of 3 expected from their stoichiometries.

3.2 RIMS of Uranium

Uranium has a strong resonance ionization signal at 591.5 nm corresponding to the two step, bound-bound transition $^5\text{L}_6 \rightarrow ^7\text{M}_7 \rightarrow ()$ followed by an ionization step, i.e., the RI signal for U^+ is produced by a single-color, three-photon absorption from the ground state of U. Thus, U atoms can be ionized by a single laser tuned to a single nominal wavelength. Power spectra, taken with the Nd:YAG-pumped dye laser at 591.5 nm, showed an initial linear dependence (slope ~ 1) on laser power for the U^+ photoionization signal with a plateau at about 6 mJ/pulse, implying that the ionization process was saturated above this pulse energy.

Figure 4 shows the optical ionization spectra of U metal obtained using the flashlamp-pumped dye laser over the wavelength range 580-607 nm. The top spectrum was obtained using Ar^+ sputter atomization, while the lower spectrum resulted from heated thermal filament atomization

ORNL-DWG 84-15518

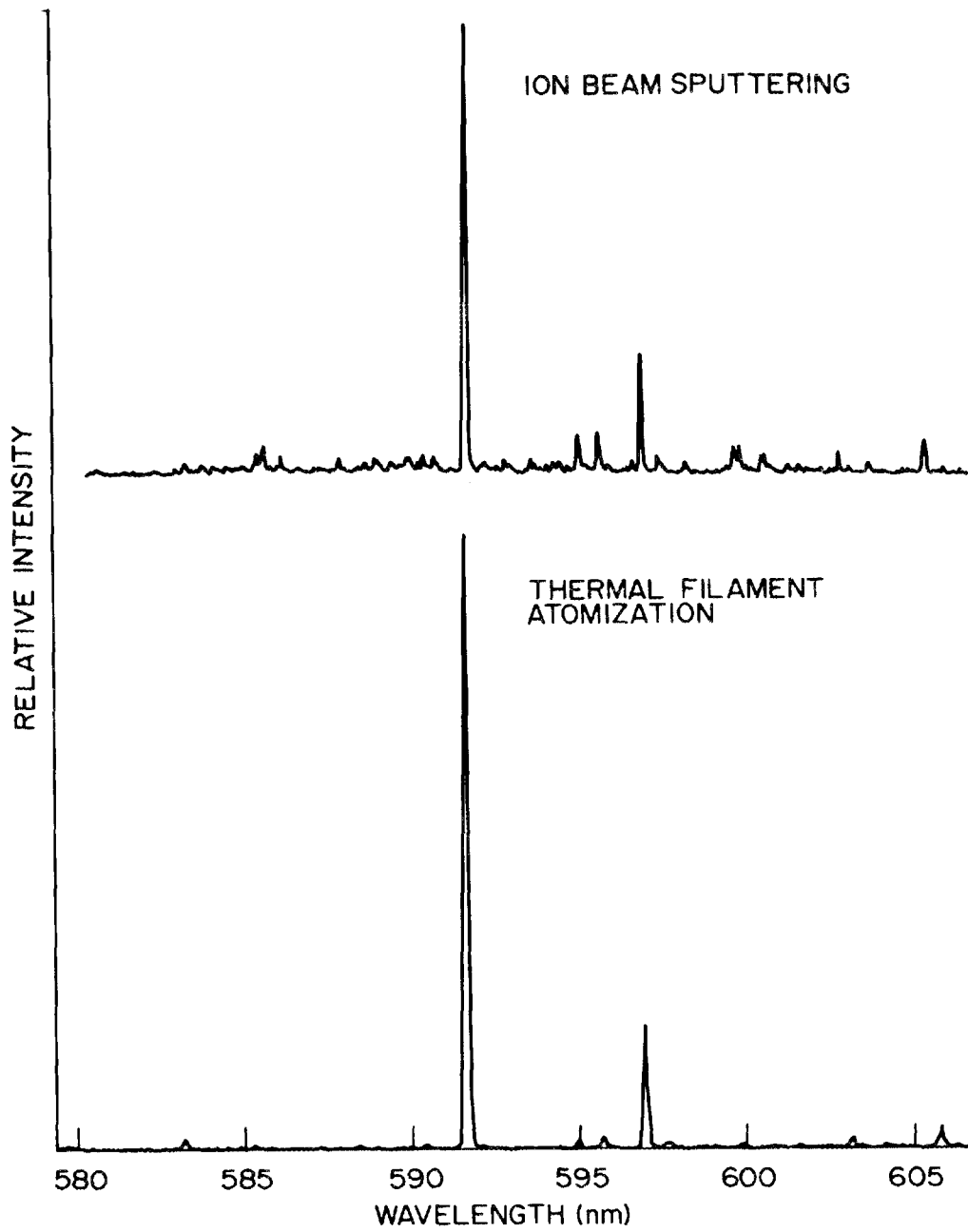


Fig. 4 Optical ionization spectra obtained with a flashlamp-pumped dye laser for ^{238}U atoms produced by ion beam sputtering (top) and thermal filament atomization (bottom).

($\sim 1500^\circ\text{C}$); the peaks observed match quite closely, with the largest signal being at 591.5 nm as expected. The peak at 596.9 nm is believed to arise from a three-photon transition originating from the $^5\text{K}_5^\circ$ excited state at 620 cm^{-1} . Figure 5 shows the optical ionization spectrum of U metal obtained with the Nd:YAG-pumped dye laser using Ar^+ sputter atomization; we were unable to monitor RI signals originating from the $^5\text{K}_5^\circ$ excited state because the pulse energy from our dye laser dropped sharply above 595 nm. As in the spectra obtained with the flashlamp-pumped dye laser, the largest signal occurred at 591.5 nm. However, many additional lines are also present; these are presumably due to the increased power per unit bandwidth in the output from the Nd:YAG-pumped dye laser.

Figure 6 shows RIMS partial mass spectra of photoions produced with the flashlamp-pumped dye laser at two different wavelengths, 591.5 and 591.3 nm, for U metal sputtered with an Ar^+ primary beam. Each spectrum contains peaks at masses corresponding to UO^+ and UO_2^+ , but the U^+ peak is only present in the spectra taken at 591.5 nm (except for a small signal for U^+ at 591.3 nm, probably from power broadening). This same effect was also seen in similar experiments using the Nd:YAG-pumped dye laser. These results suggest that uranium oxide species were sputtered and ionized via a multiphoton ionization (MPI) process.

The RIMS optical spectrum for production of UO^+ photoions from an Ar^+ -sputtered UO_2 crystal, taken with the Nd:YAG-pumped dye laser, is shown in Figure 7; similar results were obtained with the flashlamp-pumped dye laser. Their shapes essentially correspond to that for the respective laser output power curves. The signal-to-noise ratio for the UO_2^+ photoion spectra was poor, but similar broadband photoionization was observed. Nogar et al. (4) have noted that a nonresonant background in atomic RIMS can result from a broad distribution of initial internal states and a high density of excited states; direct three-photon ionizations, although not strictly resonant, may be enhanced by quasi-resonant processes for one- and two-photon levels and potentially large power-broadening effects for one-photon resonances. They suggest that spectrally broad-band, multiphoton-generated molecular ions could also be produced by similar processes.

ORNL-DWG. 87-7567

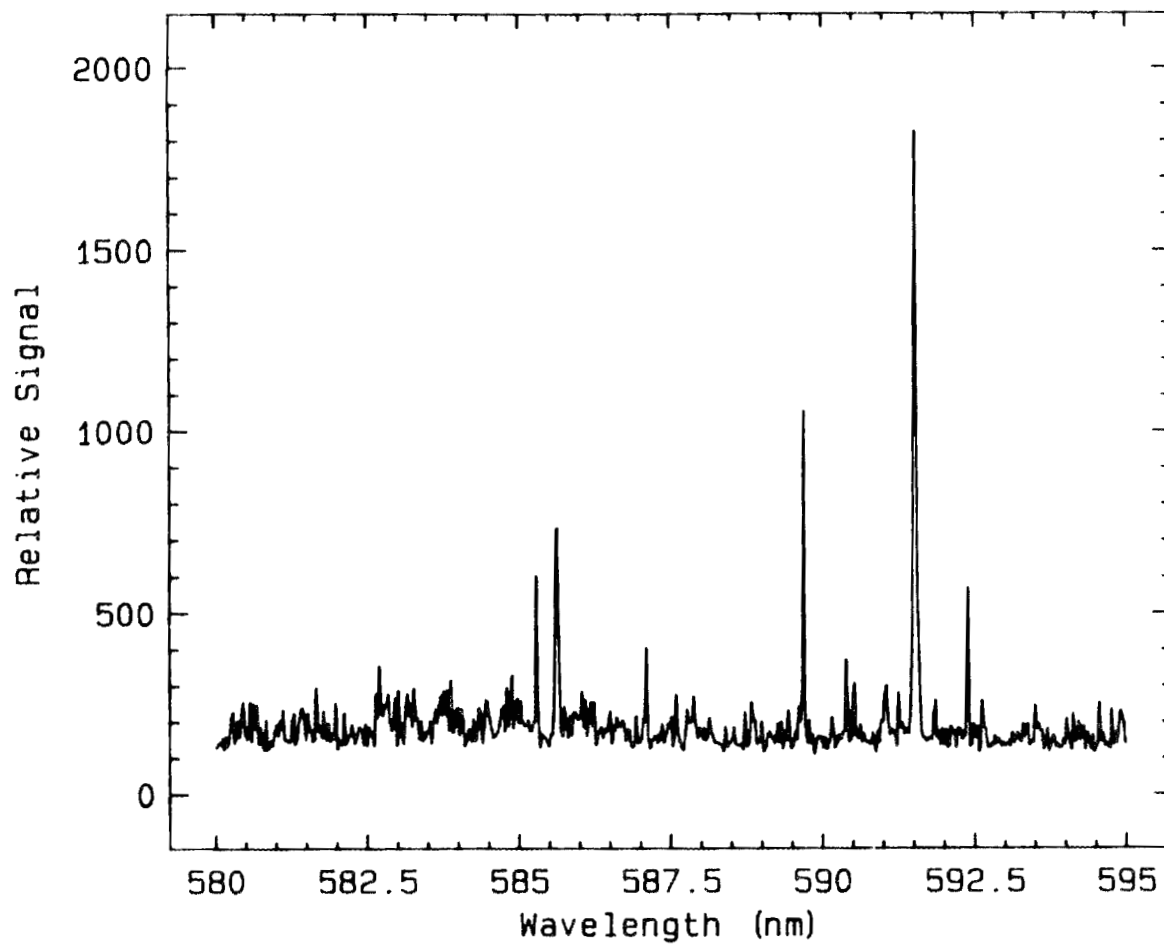


Fig. 5 Optical ionization spectrum obtained with a Nd:YAG-pumped dye laser for ^{238}U atoms produced by ion beam sputtering.

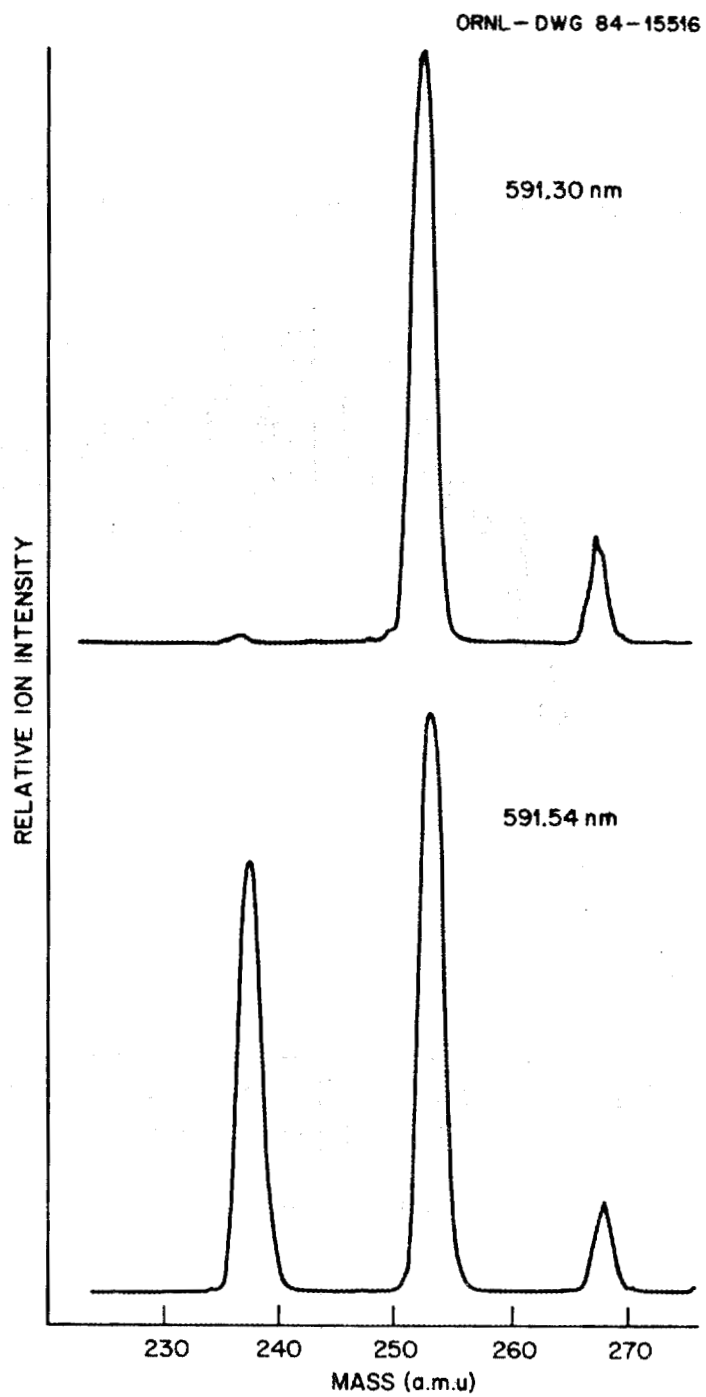


Fig. 6 Mass spectra of photoions produced via laser post-ionization of ion-beam-sputtered uranium.

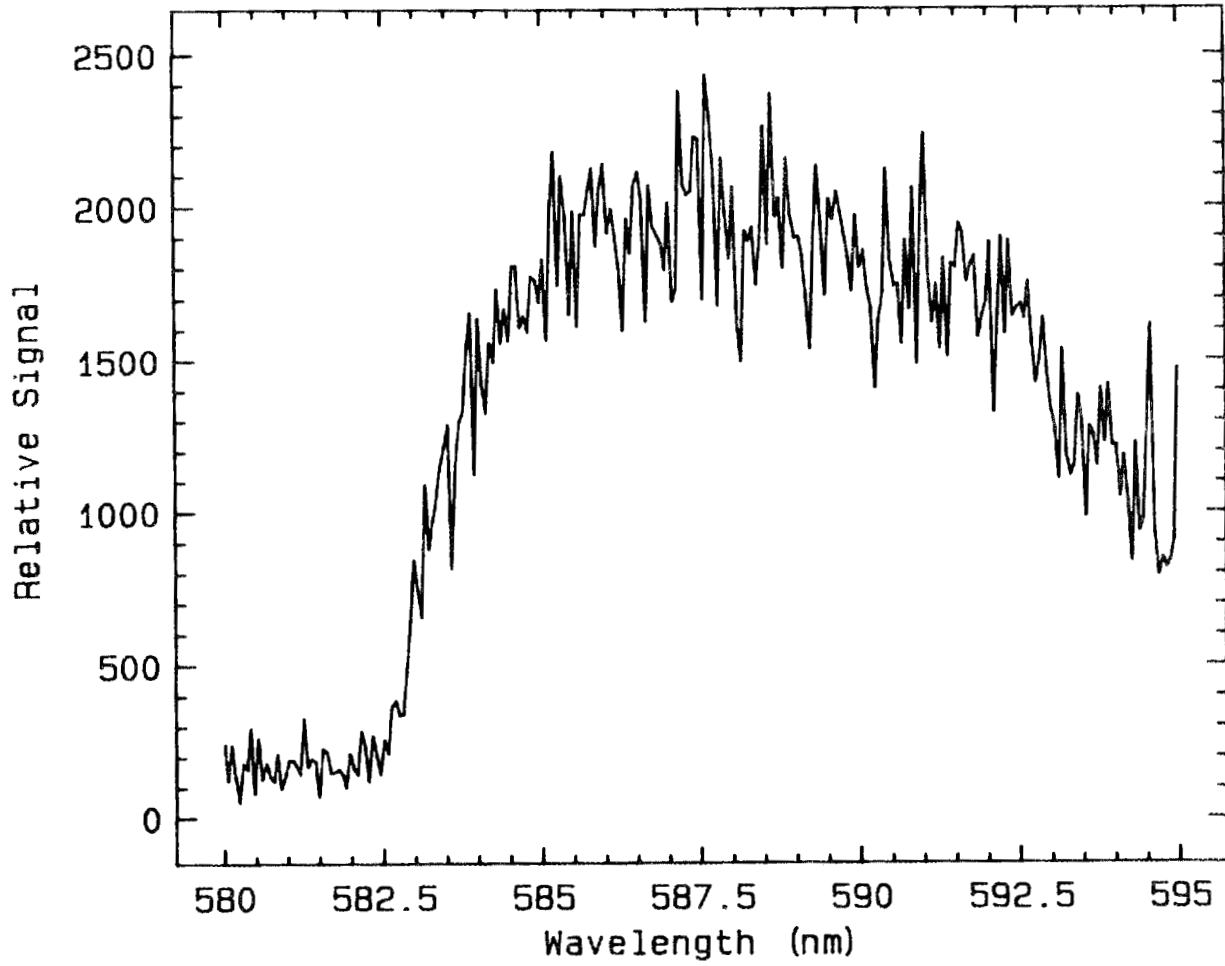
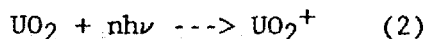
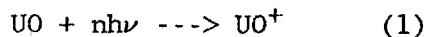
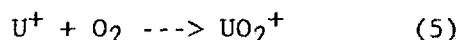
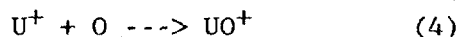
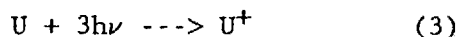


Fig. 7 Optical spectrum for production of UO^+ photoions.

This dramatic difference in wavelength sensitivity for formation of U^+ photoions in contrast with UO^+ and UO_2^+ , along with the results from Nogar et al. (4), suggests that the oxide ions are produced by photoionization of sputtered oxide molecules (eqns. 1-2)



and not by the two-step process involving RI of sputtered atoms and gas phase reaction with oxygen (eqns 3-5).



Because UO and UO_2 neutrals are photoionized at the same wavelength as U atoms, a secondary mass spectrometer was necessary in our study in order to separate by m/z the photoions produced by the laser.

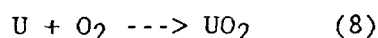
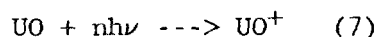
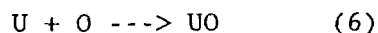
It is also interesting to note that when the U^+ photoion signal from the crystal is compared with that from U metal, it is reduced by significantly more than the factor of ~ 3 expected from the reduced U atomic density and sputter yield for the crystal. This effect was investigated further in the depth profiling study described below.

3.3 Depth Profiling

To demonstrate the effect of sample matrix on secondary ion and neutral yields, a set of depth profile measurements using SIMS and RIMS was made on a thin film UO_2/U metal sample. During the experiments a cw Ar^+ primary beam (13 nA) was rastered over a region of approximately $80 \times 100 \mu m$; the primary beam was moved to a different surface location for each new measurement. The depth profiles were made by collecting selected ion signals as a function of time. For the SIMS experiments the U^+ , UO^+ , and UO_2^+ secondary ion signals were monitored; the RIMS

measurements recorded the signals for U^+ , UO^+ , and UO_2^+ photoions produced at 591.5 nm (Nd:YAG-pumped dye laser). It should be noted that the SIMS data were obtained on a similar IMMA instrument dedicated to SIMS analyses. Figure 8 shows SIMS time (depth) profiles obtained for the secondary ions noted above; Figure 9 shows the RIMS time profiles obtained for the corresponding photoions. The slight discrepancy between elapsed times for sputtering through the oxide layer (~90 s for the SIMS experiment, ~110 s for the RIMS experiment) is due to the inability to exactly duplicate sputtering conditions in the two instruments. It should also be noted that, although the ordinate for each plot is the same, the units for the relative signals are different.

As noted previously, in the absence of any matrix effects on ion or neutral yields, the U^+ signal from the UO_2 film would be about 3 times smaller than that from U metal. Except for a high initial count rate, presumably due to surface chemisorption of oxygen-containing impurities, the secondary ion signal for U^+ changed little (down by approximately a factor of 2) going from oxide to metal. However, the photoion signal for U^+ from the UO_2 layer was over 40 times less than that from the U metal suggesting that the ground-state U atom fraction was strongly influenced by a matrix effect. The initial variation in UO^+ and UO_2^+ photoion yields is probably due to chemical changes induced in the near-surface region through long storage at ambient laboratory conditions. These effects are minimized after removal of approximately the first 30 nm and are of no consequence to the conclusions drawn in this study. Note that the signals for UO^+ and UO_2^+ photoions decreased at the transition from the UO_2 layer to the U metal surface; this also suggests that those molecular ions were primarily produced by direct photoionization of neutral oxide molecules (eqns 1-2) and not by the reaction of residual oxygen with laser-generated uranium ions (eqns 3-5), or by combination of sputtered U atoms with residual oxygen followed by photoionization (eqns 6-9).



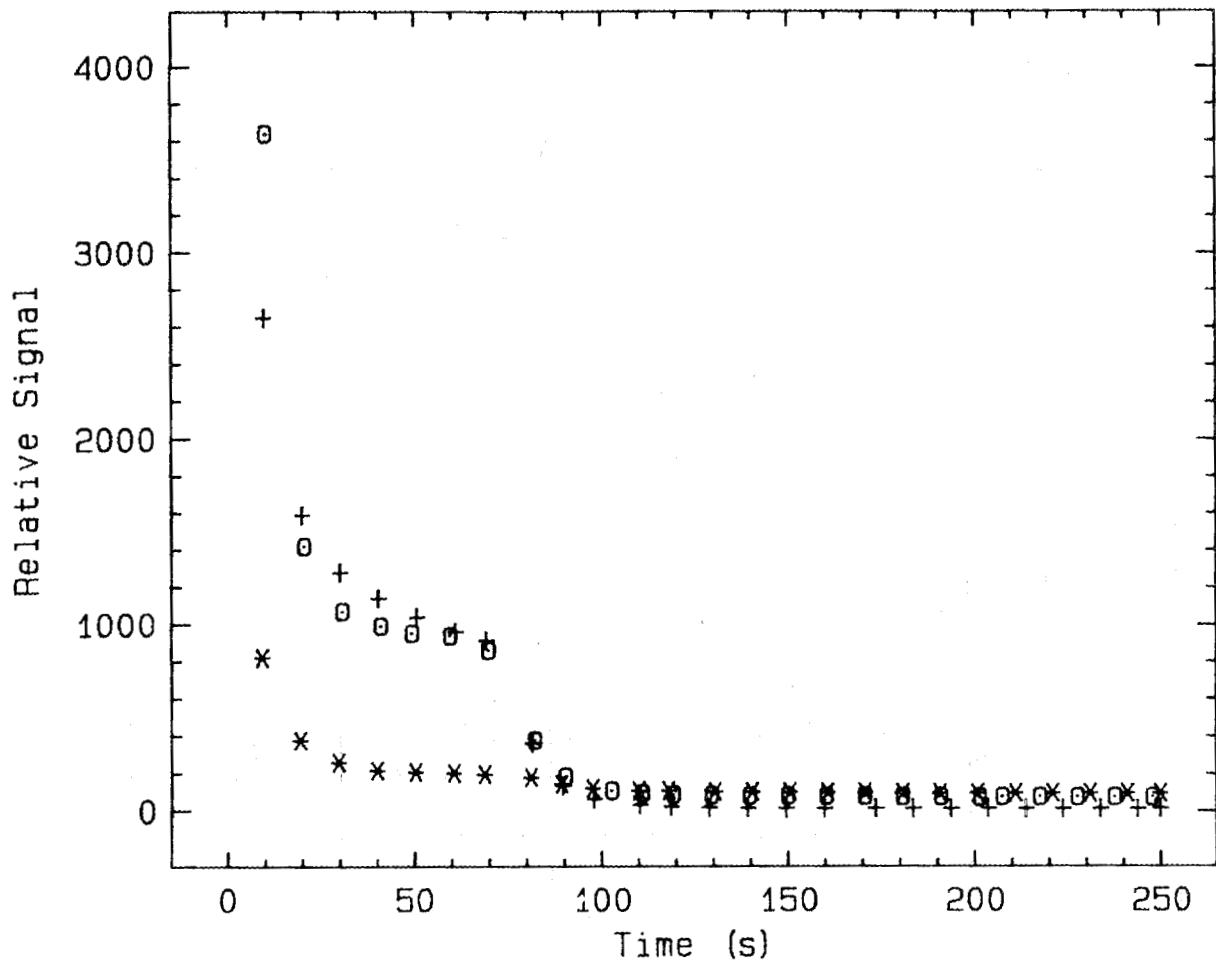


Fig. 8 Time (depth) profiles of mass-selected ions produced by ion-beam sputtering of U metal covered with a thin UO_2 film: * - U^+ , o - UO^+ , + - UO_2^+ .

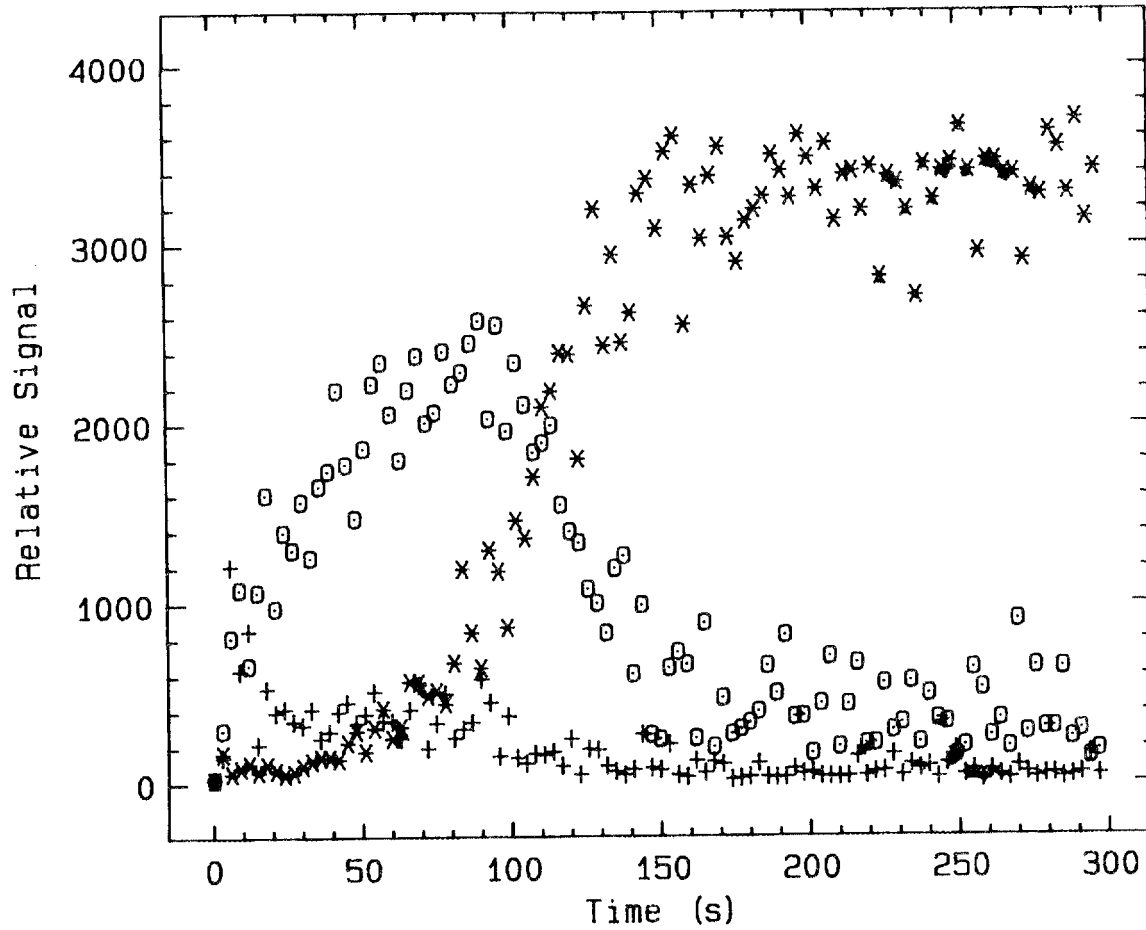


Fig. 9 Time (depth) profiles of mass-selected ions produced by laser ionization of neutrals sputtered from U metal covered with a thin UO_2 film: * - U^+ , o - UO^+ , + - UO_2^+ .

However, the data do not preclude the possibility that the molecular ions were formed by recombination of sputtered U and O atoms above the surface followed by photoionization.

3.4 Pulsed Primary Ion Beam

A set of pulse-sputtering experiments demonstrating the effect of surface contamination on neutral yields was performed. The region of the U metal surface being pulse-sputtered was initially sputter-cleaned with an 11 nA, cw Ar^+ beam focused to approximately 25 μm . Following this, the primary beam was switched to pulsed operation (10 Hz) and the photoion signal for U^+ (591.5 nm, Nd:YAG-pumped dye laser) allowed to stabilize. As the response of the photoion signal for U^+ was monitored, the Ar^+ beam was briefly switched to cw mode then returned to pulsed mode. The primary beam pulse duration was varied from 5 to 200 μs for the set of experiments, with the laser fired at the end of the gating pulse in each case. Figure 10 shows the time response of the U^+ photoion signal for two of the pulse widths used, 5 and 200 μs ; the transitions between sputter modes occurred at indicated elapsed times of 20 and 40 s. For all pulse widths there was an immediate increase in the photoion signal for U^+ upon switching to cw mode, and in each case the signal was also observed to decay at the transition back to pulsed mode. The steady state signal in pulsed mode was seen to increase with duration of sputtering by the primary beam. Figure 11 shows the time response of signals for UO^+ and UO_2^+ photoions in a pulsed-cw sequence (5 μs Ar^+ pulse) on another pre-cleaned region of the same sample. The sputter mode transition occurred at an indicated elapsed time of 50 s. As expected, the oxide photoion signals were quite evident during pulse-sputtering then declined rapidly under cw bombardment. Samarium is considerably more resistant to oxidation than U. In a similar cw-pulsed experiment the same Ar^+ beam current was used to sputter a Sm target, but the beam diameter was increased to 60 μm so that the Ar^+ current density was reduced to about 20% of that used in the U experiment. Even with the lower Ar^+ current density, a longer period (290 s) in pulse-sputter mode,

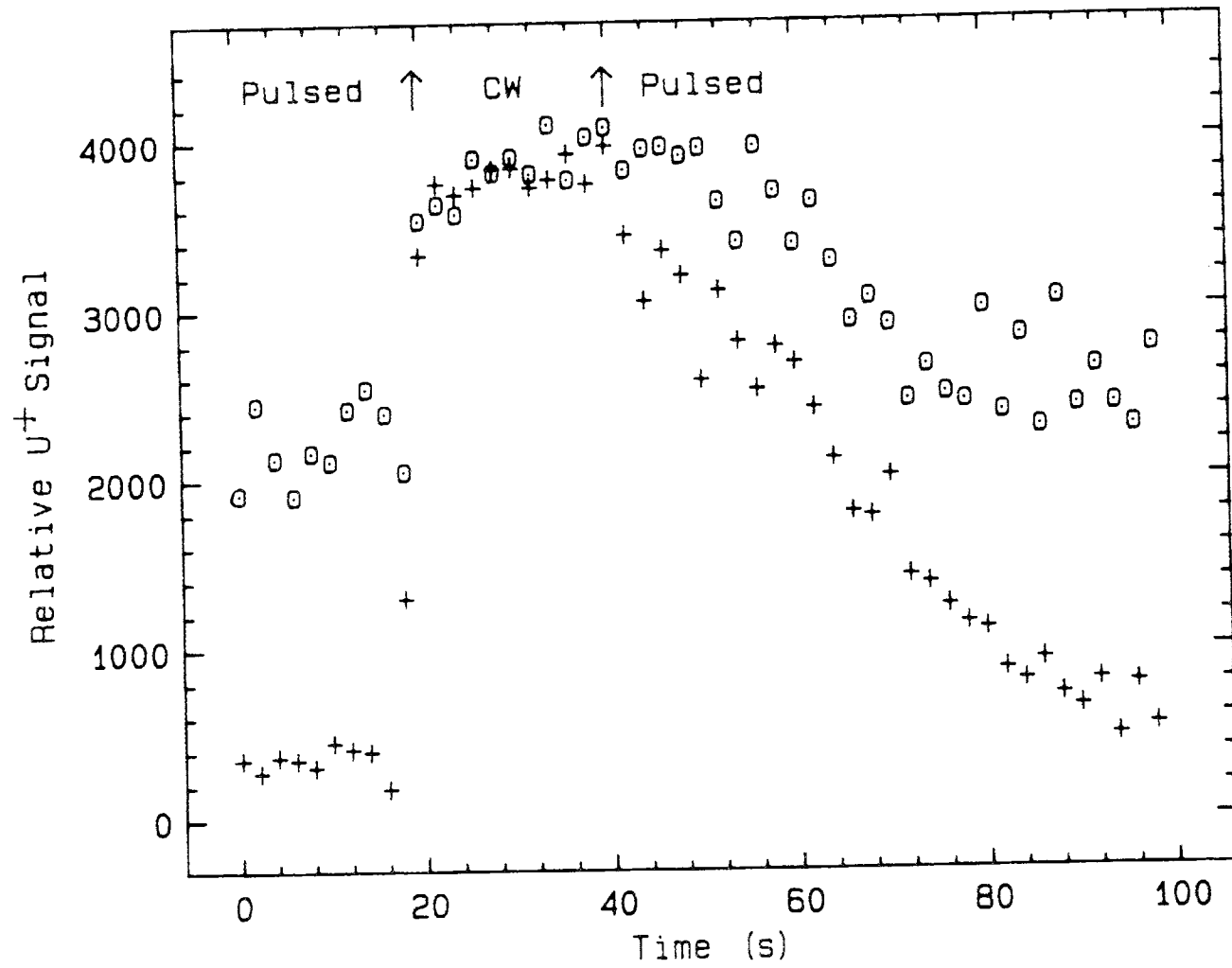


Fig. 10 Time response of the laser ionization signal for U^+ from U metal sputtered with a pulsed Ar^+ beam of varying pulse duration:
 + - 5 s, 0 - 200 s.

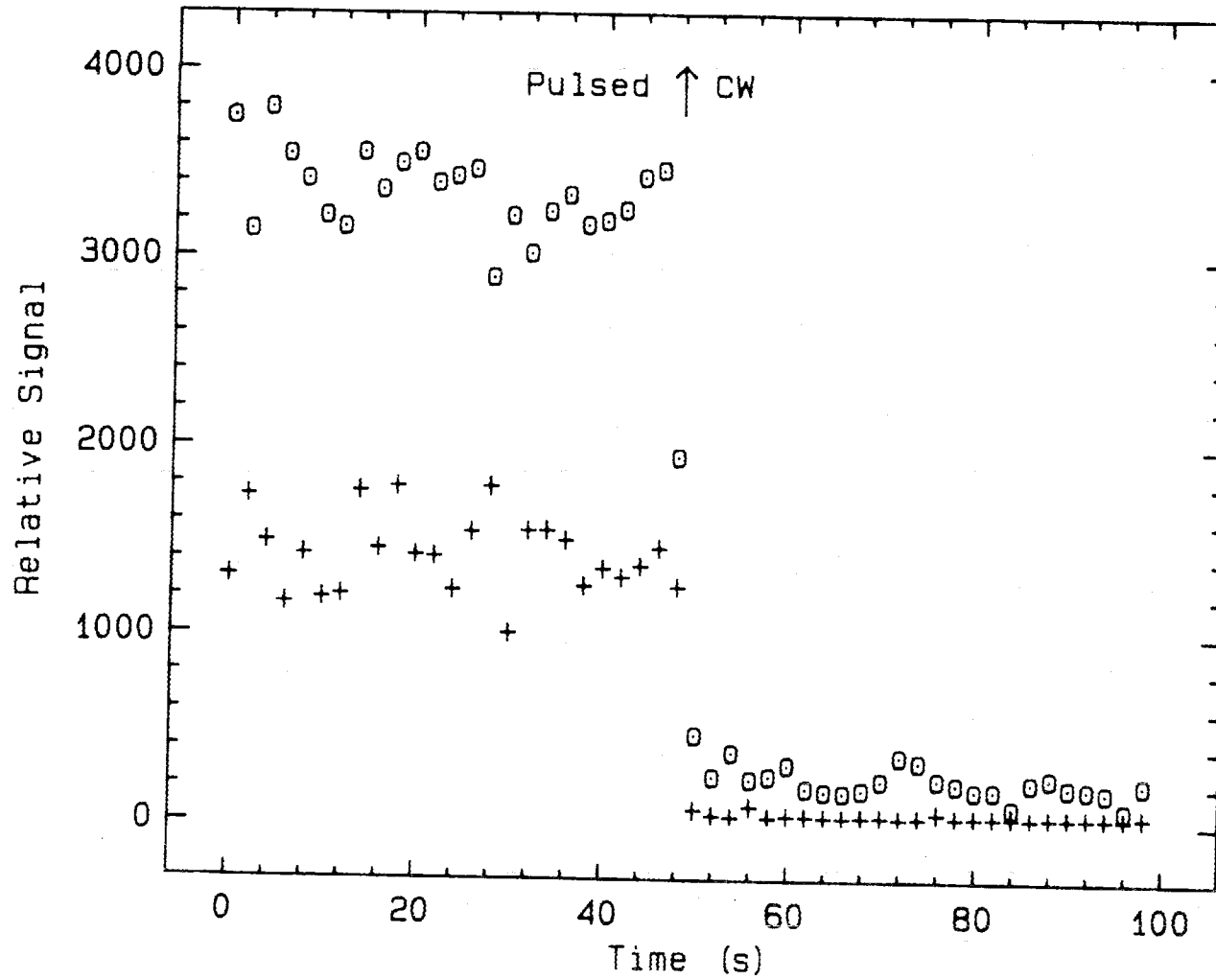


Fig. 11 Time response of the laser ionization signals for UO_2^+ from U metal alternately sputtered with a 5 s duration pulsed and cw Ar^+ beam: o - UO^+ , + - UO_2^+ .

and only a 5 μs sputter pulse, the extent of reduction (~35%) in the photoion signal for Sm^+ from cw to pulsed modes was much less severe than for U^+ . Assuming a background O_2 partial pressure of $\sim 4 \times 10^{-8}$ torr, based on a residual total pressure of $\sim 2 \times 10^{-7}$ torr, the flux of O_2 at the U surface was $1.4 \times 10^{13} \text{ cm}^{-2}\text{-s}^{-1}$ at 298 K. The Ar^+ ion flux for the 25 μm diameter, 11 nA primary ion beam was $1.4 \times 10^{16} \text{ cm}^{-2}\text{-s}^{-1}$; the duty cycle for the 5 μs , 10 Hz pulsed Ar^+ beam was 5×10^{-3} %, giving an average Ar^+ flux of $7.0 \times 10^{11} \text{ cm}^{-2}\text{-s}^{-1}$. Therefore, in cw mode the Ar^+ ion flux was much greater than the O_2 flux reaching the surface, enabling the primary beam to keep the U surface reasonably free of oxygen. In pulsed mode the average flux for Ar^+ ions was much less than for O_2 , allowing oxygen to be chemisorbed onto the U surface. The data in Figure 10 suggest that monolayer coverage occurred about 60 s after the transition from cw to pulse-sputter mode (indicated elapsed time 100 s). However, the reduction in photoion signal for U^+ at that point was greater than the factor of about 3 expected from the reduced density of surface U atoms. These experimental results suggest that the ground-state U atom fraction from sputtered U metal is sensitive to a matrix effect due to chemisorbed surface impurities. The signals for UO^+ and UO_2^+ photoions observed in pulse-sputter mode suggest that oxide formation on U metal is responsible for this matrix effect.

3.5 SIMS and RIMS Comparisons

Table I compares SIMS signals for U metal, UO_2 , and U_3O_8 samples sputtered with a 7.5 nA, cw Ar^+ beam under similar conditions. For the U metal sample, > 90% of the secondary ion signal was from U^+ . Results from the previously described pulsed primary beam experiments suggest that the contributions of UO^+ and UO_2^+ to the SIMS signal for U metal were due to chemisorption of residual oxygen-containing species and should decrease with increasing Ar^+ current density; this effect was observed in our studies. The absolute and relative yields of UO^+ and UO_2^+ secondary ions from UO_2 were greatly enhanced compared with U metal, presumably because oxygen is incorporated into the chemical lattice.

Table I. Comparison of Relative Signals for Mass-Selected Secondary and Laser-Generated Ions

Ion	SIMS			RIMS	
	U metal	UO ₂ crystal	U ₃ O ₈	U metal	UO ₂ crystal
	counts/s x 10 ³			V-s x 10 ⁻⁶	
U ⁺	93	102	750	17.0	0.39
UO ⁺	6	575	90	0.21	6.3
UO ₂ ⁺	2	895	52	---	0.57

However, the case of U₃O₈ is interesting in that the U⁺ ion appeared in greatest abundance in the SIMS spectrum despite the highly oxidized state of uranium.

Photoionization signals, produced via the Nd:YAG-pumped dye laser, from U and UO₂ samples bombarded with a 13 nA, cw Ar⁺ beam are also compared in Table I. The units for the RIMS data, V-s, result from the fact that the signal from the gated integrator is the integral of the input signal (V) over the gate duration (s). The gain factors for the detector (1.6×10^6) and preamplifier (10^5 V-A^{-1}) and the charge/ion ($1.6 \times 10^{-19} \text{ coul-ion}^{-1}$) can be combined to give a conversion factor of $2.6 \times 10^{-8} \text{ V-S-ion}^{-1}$ for calculating ions/pulse from the RIMS data. As expected for U metal, the U⁺ signal from RI of ground-state U atoms constituted the majority of the RIMS signal, with the contribution from photoionization of sputtered UO neutrals again presumed to be a function of residual chemisorbed oxygen. For the UO₂ sample, the RIMS signal for UO⁺ was considerably larger than for U⁺ and UO₂⁺. However, the actual fractions of UO and UO₂ in the sputtered neutral population may be larger than indicated by the ratios of their photoion signals with that for U. That is, the efficiency of photoionization for oxide molecules in the laser beam was unknown. No data for laser ionization on the U₃O₈ sample are shown because no photoion signals detectable above background noise were obtained under the conditions used for these comparisons. It would

appear that relatively few ground-state U atoms were sputtered from the U_3O_8 sample, and for that matter few UO and UO_2 molecules. These experiments also suggest that conventional SIMS may offer more sensitivity for the analysis of this material than SA/RIMS using this RI scheme.

Although the observed matrix effects in these experiments have been attributed to an increase in the secondary ion or molecular neutral yield, the possibility exists that the population of a low-lying excited atomic state (see above) is being increased in those instances. However, in either case the matrix effects result in reduction of the number of ground-state uranium atoms and concomitant complications for quantitative analytical measurements.

3.6 In Situ Reduction

A number of chemical reducing agents were introduced into the sputtering region in an attempt to increase the yield of sputtered atomic neutrals from oxidized forms of uranium. Three approaches were used: 1) Cesium ions were employed as a sputtering beam, 2) benzene and anhydrous ammonia were impinged on the sputter targets via a capillary jet during Ar^+ sputtering, and finally 3) Al, Ti, Zr, and C were used as substrates upon which particulate samples were dispersed prior to sputtering. During these studies, the effect on the yield of sputtered neutral particles was observed by monitoring the U^+ photoion signal. These experiments can be summarized simply by reporting that none of the approaches tried resulted in enhanced yields of sputtered U atoms from oxygen containing samples.

Direct comparison of Cs^+ sputtering with Ar^+ sputtering of U metal and its oxides was not possible in this study because the best Cs^+ current density obtainable from our ion source was about 1/15 that of the reference Ar^+ (13 nA, 25 μm dia.) beam. Cs^+ sputtering of U metal with this reduced current density always gave rise to a combined UO^+ and UO_2^+ secondary ion signal of about twice the observed U^+ secondary ion intensity. Under these conditions, no enhanced U^+ photoionization signal was observed from U metal, UO_2 , or U_3O_8 samples.

Results from the addition of gaseous reductants (NH_3 and benzene) during Ar^+ bombardment are summarized in Table II. Spectra obtained from Ar^+ sputtering of UO_2 in the presence and absence of benzene vapor show that benzene is effective in suppressing the emission of UO_2^+ . For a given benzene pressure, the Ar^+ sputter ion current density (constant beam current) could be optimized to maximize the observed U^+/UO_2^+ secondary ion ratio. If the Ar^+ sputter beam was switched to pulsed mode during the experiment (10 μs duration, 10 Hz rep. rate), the U^+/UO_2^+ ratio was observed to decrease significantly. This decrease was due to growth of the UO_2^+ signal and decrease of the U^+ signal to give essentially the same total signal level observed in the absence of benzene. This behavior suggests that O-containing species, present in the vacuum chamber, are more strongly adsorbed on the UO_2 surface and thus replace the adsorbed benzene. The photoionization signal observed for U^+ at 591.5 nm was decreased by a factor of two, whereas the photoion signals observed for UO^+ and UO_2^+ were essentially unaltered in the presence of benzene. When either U or UO_2 were exposed to NH_3 vapor, a significant reduction in U^+ RI and UO^+ , UO_2^+ MPI signals was noted.

Table II. Effect of NH_3 and C_6H_6 on Photoion and Secondary Ion Formation (Ar^+ Bombardment)

<u>Sample</u>	<u>Reductant</u>	<u>Effect on RI Signal</u>	<u>Major Ions Observed in SIMS Spectrum</u>
U	NH_3	Reduced	UN, UNH, UNH ₂ , UNH ₃ , U ₂ N, U ₂ NH ₃ , U ₂ N ₂ , U ₂ N ₂ H, U ₃ NH ₃ , U ₃ (NH ₃) ₂
U	C_6H_6	Reduced	U, UC, UC ₂ , UC ₆ H ₆ , U ₂ C, U ₂ C ₂ , U ₂ C ₃
UO_2	NH_3	Reduced	U, UH, UN, UNH, UO, UO_2 , U ₂ N, U ₂ NH, U ₂ N ₂ , U ₂ N ₂ H, U ₂ N ₃ , U ₂ N ₄
UO_2	C_6H_6	Reduced	U, UO, UC ₂ , UO_2 , UC ₆ H ₆ , U ₂ C, U ₂ O, U ₂ C ₂ , U ₂ O ₂

Finally, particulate samples of UO_2 and U_3O_8 were dispersed on reducing substrates of C, Al, Ti, and Zr. In each case co-sputtering of the sample and substrate produced an adduct ion UM^+ , where M represents the substrate element. A reduction of the observed U^+ RI signal was noted in all cases studied.

3.7 Numerical Estimates

The relative ratio of ground-state uranium atoms sputtered from U metal and oxide ($\text{U}^\circ_{\text{met}}/\text{U}^\circ_{\text{ox}}$) is estimated by direct division of the corresponding U^+ RIMS signals in Table I to be $4.4 \times 10^1 \pm 2.0 \times 10^1$. A detailed consideration of extraction efficiency, cw vs. pulse-sputtering, and spatial overlap between sputtered atoms and the photon field, along with the conversion factor for the Table I data, allow us to estimate within approximately an order of magnitude the number of ground-state U atoms sputtered relative to the number of secondary U^+ ions ejected, ($\text{U}^\circ_{\text{Ar}}/\text{U}^+_{\text{Ar}}$).

First, the ion extraction and transmission efficiencies for secondary and laser-generated ions are taken to be the same after instrumental conditions are optimized for SIMS and RIMS measurements, respectively. Second, all ground-state U atoms intersected by the laser beam are assumed to be ionized as suggested by the plateau above 6 mJ/pulse in the U^+ RIMS signal versus laser pulse energy data. Note that this condition is not necessary in order to compare the relative populations of ground-state U atoms sputtered from the U metal and UO_2 samples because the same RI process, laser power, and primary ion current were used for each. Third, the count rate for U^+ secondary ions is directly proportional to primary ion current, i.e., the secondary ion count rates in Table I, measured for 7.5 nA Ar^+ ion current, can be linearly extrapolated to 13 nA as was used in the RIMS measurements. Data from our IMMA instrument dedicated to SIMS analyses showed linearity of SIMS signals for U^+ , UO^+ , and UO_2^+ in this Ar^+ current range. Fourth, the photoion signal for U^+ using cw-sputtering can be related to that using pulse-sputtering, i.e., neglecting chemisorbed surface impurity effects, at what sputter-pulse

duration does the RIMS signal become equal to that with cw-sputtering. Results from Kimock et al. (5) indicate that the photoion signal from pulse-sputtering should equal that from cw-sputtering for pulse widths $> 5 \mu\text{s}$. Our experiments with Ar^+ on Sm metal showed a small decrease in the photoion signal for Sm^+ upon switching from cw to $5 \mu\text{s}$ pulse-sputtering. However, this decrease was probably due to surface coverage by residual oxygen as discussed for the uranium metal pulse-sputtering experiments. Therefore, neglecting the matrix effect from chemisorbed oxygen, the photoion signal for U^+ with $5 \mu\text{s}$ pulse-sputtering is assumed equal to that with cw-sputtering. Fifth, for a given sputter-pulse duration, the number of sputtered ground-state U atoms can be obtained from the number of U^+ photoions in the corresponding RIMS signal. That is, knowing the sputter-pulse duration, what fraction of sputtered ground-state U atoms are intersected (and ionized) by the laser beam. Kimock et al. (5) also calculated the fraction of neutrals intersected by the laser beam during a $5 \mu\text{s}$ sputter pulse to be approximately 0.28. Thus, with these assumptions, the number of ground-state U atoms ejected with a $5 \mu\text{s}$ sputter-pulse can be obtained by dividing the number of laser-generated ions from cw-sputtering by the factor 0.28. Note that this is different from the total number of U atoms (which are ejected as neutral and charged atoms, polyatomics, clusters, etc.) calculated from the sputter yield data. The number of secondary ions generated in such a sputter-pulse can easily be calculated from secondary ion count rates by multiplication. Given these caveats, the ratio of ground-state uranium atoms to ions ($\text{U}^0_{\text{Ar}}/\text{U}^+_{\text{Ar}}$) for cw, Ar^+ ion sputtering from U metal and UO_2 are estimated from the Table I data to be 3×10^3 and 6×10^1 , respectively.

The absolute efficiency for SA/RIMS can be defined as the number of U^+ photoions detected/U atoms sputtered. Because the optical pulse duration for the flashlamp-pumped dye laser was $\sim 1 \mu\text{s}$, the number of photoions produced by a single laser shot could be estimated by counting ion pulses on a fast oscilloscope. Approximately 100 U^+ photoions/laser shot were produced when a 21 nA, cw Ar^+ beam was used to sputter a U metal sample. Therefore, the absolute efficiency for the flashlamp-pumped laser, neglecting duty factor considerations and assuming a

sputter yield of 5.3 , was about 1.5×10^{-4} . In another independent experiment using the Nd:YAG-pumped dye laser, the U^+ photoion signal from a U metal sample sputtered with a 500 ns duration, 9 nA Ar^+ beam was estimated to contain about 135 ions. The absolute efficiency for SA/RIMS from this data, again assuming a sputter yield of 5.3, was estimated to be 9×10^{-4} . These data indicate that the Nd:YAG-pumped dye laser gave an improvement in absolute efficiency of approximately a factor of 6 over the flashlamp-pumped dye laser.

For a similar pulse-sputtering experiment, Kimock et al. (5) calculated the fraction of neutrals intersected by the laser beam during a 500 ns sputter pulse to be approximately 0.68. If the absolute efficiency is taken as the product of the spatial overlap factor and the transmission/detection efficiency for photoions, then the transmission/detection efficiency for our instrument is about 1.3×10^{-3} .

The transmission/detection efficiency and neutral-to-ion ratio estimated above can be combined with the U^+ secondary ion data to perform a particle ejection rate comparison with the total desorbed material estimated from sputter yield data. Because the ionization efficiencies for sputtered molecular neutrals are not known, the calculation is most significant for U metal where U° and U^+ dominate the sputtered particle yield. Since the population of species desorbed from U metal in turn is dominated by U° , the sputtered U^+ secondary ions can be neglected. Using the U^+ secondary ion data from Table I (9.3×10^4 c/s) and the calculated transmission/detection efficiency, the U^+ secondary ion sputter rate is 7.0×10^7 s⁻¹. Multiplying by the U°_{Ar}/U^+_{Ar} ratio estimated above, the ejection rate for U° is 2.1×10^{11} s⁻¹. This compares well with the desorbed particle rate for a 7.5 nA Ar^+ beam (sputter yield 5.3) of 2.5×10^{11} s⁻¹.

4. Conclusion

At one time high efficiency, laser post-ionization of sputtered atomic species was thought to offer the possibility for quantitative surface analysis. Such studies performed under ultra-high vacuum conditions using inert gas sputtering of metallic targets showed that in some cases quantitative analysis could be accomplished without matrix effects (6). Unfortunately, these laboratory conditions do not exist for the analysis of all samples. The industrially generated, particulate emissions for many reactive metals of environmental significance are often not found in the metallic state; they form a variety of compounds through reaction with the environment. This work clearly indicates that the population of desorbed neutrals above such sample surfaces may not always be directly representative of its composition. Just as chemistry in the sputtering region can dominate relative ion yields in SIMS experiments, it may also control the relative sputtered neutral yield detected by RIMS. The possibility that the desorbed neutral fraction can be partitioned amongst a variety of species will complicate the task of relating laser-generated ion abundances to the actual composition of the sputtered surface.

References

- (1) Morabito, J. M.; Lewis, R. K. Anal. Chem. 1973, 45, 869-880.
- (2) Goeringer, D. E.; Christie, W. H.; McKown, H. S.; Donohue, D. L. ORNL/TM-9949 1986.
- (3) Liebl, H. J. Appl. Phys. 1967, 38, 5277-5283.
- (4) Nogar, N. S.; Downey, S. W.; Miller, C. M. Anal. Chem. 1985, 57, 1144-1147.
- (5) Kimock, F. M.; Baxter, J. P.; Pappas, D. L.; Kobrin, P. H.; Winograd, N. Anal. Chem. 1984, 56, 2782-2791.
- (6) Moore, L. J. 30th Ann. Conf. Mass Spec. Allied Top. Workshop Report, "Laser Mass Spectrometry for the Production and Measurement of Inorganic Ions" 1982.

Internal Distribution

1. L. K. Bertram
2. J. A. Carter
3. W. H. Christie
4. D. E. Goeringer
5. S. A. Levin, ORGDP
6. W. D. Shults
7. D. W. Swindle, ORGDP
8. R. L. Walker
9. A. Zucker
10. Central Research Library
11. Document Reference Section
12. ORNL Patent Office
- 13-14. Laboratory Records Department
15. Laboratory Records Department-RC

External Distribution

16. J. B. Gerardo, Sandia National Laboratories, P. O. Box 5800, Albuquerque, NM 87115
17. P. D. Gildea, Sandia National Laboratories, P. O. Box 969 Livermore, CA 94550
18. A. L. Boni, Savannah River Laboratory, P. O. Box 1001, Aiken, SC 29801
19. Max Koontz, DP-331.1, DOE, Washington, DC 20585
20. David Dingee, DP-331.1, DOE, Washington, DC 20585
21. E. P. Steinberg, Argonne National Laboratory, Argonne, IL 60439
22. Paul R. Guthals, Los Alamos National Laboratory, MS 5000, Los Alamos, NM 87545
23. J. W. Hadley, Lawrence Livermore National Laboratory, Livermore, CA 94550
24. N. E. Ballou, Pacific Northwest Laboratory, P. O. Box 999, Richland, WA 99352
25. Assistant Manager for Energy Research and Development, Department of Energy, Oak Ridge Operations Office, Oak Ridge, TN 37831
- 26-55. Technical Information Center, Oak Ridge, TN 37831

